Journal of Computational Applied Mechanics 2025, 56(4): 720-736

DOI: 10.22059/jcamech.2025.397650.1525

RESEARCH PAPER

Thermomechanical deformation in a micropolar thermoviscoelastic solid under the Moore-Gibson-Thompson heat equation with non-local and hyperbolic two-temperature effects

Kunal Sharma [a,*], Marin Marin [b,c,†], Rajneesh Kumar [d,‡]

[a] *Cheminde Chandieu 25, 1006 Lausanne, Switzerland*
[b] *Department of Mathematics and Computer Science, Transilyania University of Brasov,500036 Brasov, Romania*
[c] *Academy of Romanian Scientists, Ilfov Street, 3, 050045 Bucharest, Romania*
[d] *Department of Mathematics, Kurukshetra University, Kurukshetra 136119, Haryana, India*

Abstract

This study addresses an axisymmetric problem within the framework of micropolar thermoviscoelasticity, governed by the Moore-Gibson-Thompson (MGT) heat conduction equation. The analysis incorporates non-local elasticity and hyperbolic two-temperature (HTT) effects under applied mechanical loading. By introducing appropriate potential functions, the governing system is reformulated into a dimensionless form and solved using Laplace and Hankel transform techniques. Boundary conditions involving a normally distributed mechanical force and a ramp-type thermal input are considered to examine their impact. Analytical expressions for displacements, stress components, tangential couple stress, conductive temperature, and thermodynamic temperature are derived in the transformed domain and subsequently recovered using a numerical inversion method. Graphical representations illustrate how variations in viscosity, non-locality, and HTT parameters influence thermal and mechanical responses. Special cases are also examined to validate the model's generality. This research holds relevance for industrial applications in steel manufacturing and petroleum engineering, as well as in geomechanical modeling, particularly in understanding stress and temperature behavior during seismic activities.

Keywords: Micropolar Thermoviscoelasticity; Moore-Gibson-Thompson Equation; Hankel transform techniques; Hyperbolic Two-Temperature Model; Analytical Thermomechanical Modeling; Seismic Thermoelastic Simulation.

1. Introduction

Modeling the behavior of thermoviscoelastic materials continues to be a focal point in materials science and

* Corresponding author. *E-mail address:* kunal.nit90@gmail.com

† Corresponding author. *E-mail address:* m.marin@unitbv.ro

‡ Corresponding author. *E-mail address:* rajneesh_kuk@rediffmail.com

engineering, where researchers seek robust frameworks to accurately capture thermomechanical responses. Among the significant advancements, the two-temperature (TT) theory introduced by Chen and Gurtin [1], and later expanded by Chen et al. [2], distinguishes between the thermodynamic temperature associated with mechanical interactions and the conductive temperature. Building upon this, Youssef [3] and Youssef and El-Bary [4] proposed generalized forms, including the hyperbolic two-temperature (HTT) theory, which further improve the classical models Hobiny, Abbas, and Marin, [5] demonstrated the impact of HTT on waves behavior in a semiconductor material containing spherical cavity.

Eringen and Edelen [6] for small scale-structure problems introduced a non-local continuum mechanics theory. In contrast to local elasticity theory, which only considers the strain at a single point, nonlocal elasticity theory consider strain at every point in the medium. Micropolar elasticity, formulated by Eringen [7], allows for the consideration of micro-rotational effects and couple stresses, making it suitable for small-scale and high-frequency mechanical analyses. Marin [8] presented weak solution in elasticity of dipolar porous materials. Sharma, and Marin, [9] investigated reflection and transmission problem in micropolar thermoelastic with imperfect boundaries.

The classical coupled theory of thermoelasticity has been unable to effectively predict the outcomes during the examination of microstructures. As a result, generalized theories of thermoelasticity have played a crucial role in the analysis of this type of issue. The Moore-Gibson-Thomson model of generalized thermoelasticity, developed by Quintanilla [10] is one such model and has been widely used and studied by various researchers. Marin et al. [11] provided theoretical foundations for the influence domain in dipolar materials by using MGT heat equation. Contributions by Sharma and Khator [12, 13] addressed energy generation and grid design using renewable sources. Bhatti, M.M., et al., [14], and Zeeshan, A., et al., [15] examined some significant problems of nano fluid under MHD response. Abouelregal, A.E., et al. [16] explored the problem of a thermo-piezoelectric functionally graded rotating rod by using MGT model. Sharma, Marin and Altenbach [17] investigated elastodynamics interactions in thermoelastic diffusion under non-local and phase lags. Marin et.al., [18] examined fundamental solution and Green's function in photothermelastic under MGT model.

The current study aims to explore the combined influence of viscosity, non-local effects, and the HTT model under the MGT heat equation. A deformation problem is analyzed in a micropolar thermoviscoelastic solid subjected to a normally distributed force and a ramp-type thermal input. The system of governing equations is solved using integral transforms, and results are numerically inverted and plotted to highlight the physical implications. Some unique cases are also listed.

2. Fundamental Equations

The field equations and constitutive relations in absence of body forces, body couples and heat source (Youssef and El-Bary [4], Eringen [7] and Quintanilla [10]) are as follows:

$$(\lambda_0+\mu_0)\nabla(\nabla.\vec{u})+(\mu_0+\kappa_0)\nabla^2\vec{u}+\kappa_0(\nabla\times\vec{\phi})-\gamma_1\nabla T=\rho\left(1-{\xi_1}^2\nabla^2\right)\frac{\partial^2\vec{u}}{\partial t^2}, \tag{1}$$

$$(\alpha_0+\beta_0)\nabla\left(\nabla.\vec{\phi}\right)+\gamma_0\nabla^2\vec{\phi}+\kappa_0(\nabla\times\vec{u})-2\kappa_0\vec{\phi}=\rho\hat{j}\left(1-{\xi_2}^2\nabla^2\right)\frac{\partial^2\vec{\phi}}{\partial t^2}, \tag{2}$$

$$\left(1+\tau_0\frac{\partial}{\partial t}\right)\left[\rho C_e\frac{\partial^2 T}{\partial t^2}+\gamma_1 T_0\frac{\partial^2}{\partial t^2}(\nabla.\vec{u})\right]=K_1^*\nabla^2\dot{\varphi}+K^*\nabla^2\varphi, \tag{3}$$

$$m_{ij}=\alpha_0\phi_{r,r}\delta_{ij}+\beta_0\phi_{i,j}+\gamma_0\phi_{j,i}, \tag{4}$$

$$t_{ij}=\lambda_0 u_{r,r}\delta_{ij}+\mu_0\left(u_{i,j}+u_{j,i}\right)+\kappa_0\left(u_{j,i}-\varepsilon_{ijr}\phi_r\right)-\gamma_1 T\delta_{ij}, \tag{5}$$

$$\ddot{T}=\ddot{\varphi}-\beta^*\nabla^2\varphi, \tag{6}$$

and

$$\lambda_0=\lambda\left(1+Q_1\frac{\partial}{\partial t}\right),\qquad \mu_0=\mu\left(1+Q_2\frac{\partial}{\partial t}\right),\quad \kappa_0=\kappa\left(1+Q_3\frac{\partial}{\partial t}\right),\quad \alpha_0=\alpha\left(1+Q_4\frac{\partial}{\partial t}\right),$$

$$\beta_0=\beta\left(1+Q_5\frac{\partial}{\partial t}\right),\qquad \gamma_0=\gamma\left(1+Q_6\frac{\partial}{\partial t}\right),$$

where

$$(Q_1, Q_2, Q_3, Q_4, Q_5, Q_6) = (\frac{\lambda^v}{\lambda}, \frac{\mu^v}{\mu}, \frac{\kappa^v}{\kappa}, \frac{\alpha^v}{\alpha}, \frac{\beta^v}{\beta}, \frac{\gamma^v}{\gamma})$$

being micropolar viscoelastic relaxation times, also $\lambda^v, \mu^v, \kappa^v, \alpha^v, \beta^v, \gamma^v$ are viscoelastic constants, λ, μ are Lame's constants, $\kappa, \alpha, \beta, \gamma$ are micropolar constants, $\vec{u}$ is displacement vector, $\vec{\phi}$ is microrotation vector, $\gamma_1 = (3\lambda_0 + 2\mu_0 + \kappa_0)\alpha_t$, α_t is coefficient for linear thermal expansion, m_{ij} is component of couple stress tensor, K_1^* is thermal conductivity, t is time, φ is conductive temperature, t_{ij} are stress components, T is thermodynamic temperature, τ_0 is relaxation time, ρ is density, C_e is specific heat, δ_{ij} is Kronecker delta, β^* is hyperbolic two-temperature parameter, T_0 is reference temperature, ε_{ijr} is alternating tensor, $K^* = \frac{(\lambda_0+2\mu_0)C_e}{4}$ is rate of the thermal conductivity, ξ_1 and ξ_2 are non-local parameters, ∇^2 is Laplacian operator.

Following cases arises:
(i) For L-S theory (1967) [15]: $K^* = 0$,
(ii) For Green-Naghdi–II theory (GN II) (1993) [25]: $K_1^* = \tau_0 = 0$,
(iii) For Green-Naghdi–III theory (GN III) (1992) [14]: $\tau_0 = 0$.

3. Formulation and solution of Problem

We consider an axisymmetric problem in homogeneous, isotropic micropolar thermoviscoelastic half-space under MGT heat equation with non-local and HTT in the undeformed state T_0. A cylindrical coordinate system (r, θ, z) with axis of symmetry as z-axis pointing vertically downward into the medium is considered. For two-dimensional problem, we assume the components of displacement and microrotation vector as:

$$\vec{u} = (u_r, 0, u_z) \text{ and } \vec{\phi} = (0, \phi_\theta, 0). \quad (7)$$

Since we had taken symmetry about z-axis, so all the partial derivatives with respect to the variable θ **would be zero.**

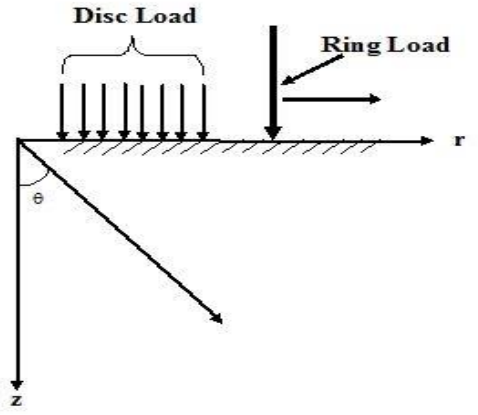

Figure 1: Schematic representation of the problem

For further simplifications, following dimensionless quantities are taken as

$$(r', z', u_r', u_z', \xi_1', \xi_2') = \frac{\omega_1}{c_1}(r, z, u_r, u_z, \xi_1, \xi_2), \qquad \phi_\theta' = \frac{\rho {c_1}^2}{\gamma_1 T_0}\phi_\theta, \quad (\varphi', T') = \frac{1}{T_0}(\varphi, T),$$
$$(\tau_0', t') = \omega_1(\tau_0, t), \beta^{*'} = \frac{1}{c_1^2}\beta^*, \ (t_{zz}', t_{zr}') = \frac{1}{\gamma_1 T_0}(t_{zz}, t_{zr}), \qquad m_{z\theta}' = \frac{\omega_1}{\gamma_1 c_1 T_0} m_{z\theta}, \quad (8)$$

where

$$c_1^2 = \frac{\lambda+2\mu+\kappa}{\rho}, \ \ \omega_1 = \frac{\rho c_1^2 C_e}{\kappa_1^*}.$$

Using Helmholtz decomposition, the displacement components u_r, u_z and micro-rotational component ϕ_θ related to the scalar potential functions are taken as

$$u_r = \frac{\partial \psi_1}{\partial r} + \frac{\partial^2 \psi_2}{\partial r \partial z}, \quad u_z = \frac{\partial \psi_1}{\partial z} - \left(\frac{\partial^2}{\partial r^2} + \frac{1}{r}\frac{\partial}{\partial r}\right)\psi_2, \quad \phi_\theta = -\frac{\partial \Gamma}{\partial r}. \tag{9}$$

Equations (1) - (3) reduce to the following form after using equations (7) - (9) as:

$$b_1^0 \frac{\partial(\nabla^2\psi_1)}{\partial r} + b_2^0\left(\frac{\partial(\nabla^2\psi_1)}{\partial r} + \frac{\partial^2(\nabla^2\psi_2)}{\partial r \partial z} - \frac{1}{r^2}\left(\frac{\partial \psi_1}{\partial r} + \frac{\partial^2 \psi_2}{\partial r \partial z}\right)\right) + b_3^0 \frac{\partial^2 \Gamma}{\partial z \partial r} - b_4^0 \frac{\partial T}{\partial r} = \tag{10}$$
$$\left(1 - {\xi_1}^2 \nabla^2\right)\frac{\partial^2}{\partial r^2}\left(\frac{\partial \psi_1}{\partial r} + \frac{\partial^2 \psi_2}{\partial r \partial z}\right),$$

$$b_1^0 \frac{\partial(\nabla^2\psi_1)}{\partial z} + b_2^0 \nabla^2\left(\frac{\partial \psi_1}{\partial z} + \frac{\partial^2 \psi_2}{\partial r^2} - \frac{1}{r}\left(\frac{\partial \psi_2}{\partial r}\right)\right) - b_3^0\left(\frac{\partial^2 \Gamma}{\partial r^2} + \frac{1}{r}\frac{\partial \Gamma}{\partial r}\right) - b_4^0 \frac{\partial T}{\partial z} =$$
$$\left(1 - {\xi_1}^2 \nabla^2\right)\frac{\partial^2}{\partial t^2}\left(\frac{\partial \psi_1}{\partial z} - \frac{\partial^2 \psi_2}{\partial r^2} - \frac{1}{r}\frac{\partial \psi_2}{\partial r}\right), \tag{11}$$

$$b_5^0\left(\nabla^2 - \frac{1}{r^2}\right)\frac{\partial \Gamma}{\partial r} - b_6^0 \frac{\partial(\nabla^2\psi_2)}{\partial r} - b_7^0 \frac{\partial T}{\partial r} = \left(1 - {\xi_2}^2 \nabla^2\right)\frac{\partial^3 \Gamma}{\partial t^2 \partial r}, \tag{12}$$

$$\left(1 + \tau_0 \frac{\partial}{\partial t}\right)\left(\frac{\partial^2 T}{\partial t^2} + b_8^0(\nabla^2 \psi_1)\right) = \nabla^2 \dot{\psi_2} + b_9^0 \nabla^2 \psi_2, \tag{13}$$

Making use of (7) - (8) in (4) - (5), yield

$$t_{zz} = b_{10}^0 \frac{\partial u_z}{\partial z} + b_{11}^0\left(\frac{\partial u_r}{\partial r} + \frac{u_r}{r}\right) - T, \tag{14}$$
$$t_{zr} = b_{12}^0 \frac{\partial u_r}{\partial z} + b_{13}^0 \frac{\partial u_z}{\partial r} - b_{14}^0 \phi_\theta, \tag{15}$$
$$m_{z\theta} = b_{15}^0 \frac{\partial \phi_\theta}{\partial z}, \tag{16}$$

where $b_j^0 \ (j = 1 - 15)$ and ∇^2 are given in Appendix I.

We define Laplace transform and Hankel transform as:

$$\bar{g}(r, z, p) = L\{g(r, z, t)\} = \int_0^\infty g(r, z, t) e^{-pt} dt, \tag{17}$$

and

$$\hat{g}(\chi, z, s) = H_n\{\bar{g}(r, z, p)\} = \int_0^\infty r\bar{g}(r, z, p) J_n(\chi r) dr, \tag{18}$$

where p denotes Laplace parameter, χ represents Hankel's parameter and J_n is Bessel function of first kind of order n.

Appling Laplace transform and Hankel transform defined by (17) - (18) on (6), we get

$$\hat{T} = \hat{\varphi} - \varsigma\left(\frac{d^2}{dz^2} - \chi^2\right)\hat{\varphi},$$

where $$\varsigma = \begin{cases} 0, & \text{for one temperature,} \\ a, & \text{for TT,} \\ \frac{\beta^*}{p^2}, & \text{for HTT.} \end{cases} \tag{19}$$

Using equations (17) - (19) on equations (10) - (13) and after simplification, we get

$$\left(\frac{d^4}{dz^4} - D_{01}\frac{d^2}{dz^2} + D_{02}\right)\left(\hat{\varphi}, \hat{\psi}_1\right) = 0, \tag{20}$$

$$\left(\frac{d^4}{dz^4} - D_{03}\frac{d^2}{dz^2} + D_{04}\right)\left(\hat{\Gamma}, \hat{\psi}_2\right) = 0, \tag{21}$$

where symbols are defined in Appendix-II.

The roots of characteristic equation

$$\left(\frac{d^4}{dx_3{}^4} - D_{01}\frac{d^2}{dx_3{}^2} + D_{02}\right) = 0,$$

are $\pm\lambda_i (i = 1,2)$ and the roots of characteristic equation

$$\left(\frac{d^4}{dx_3{}^4} - D_{03}\frac{d^2}{dx_3{}^2} + D_{04}\right) = 0$$

are $\pm\lambda_j (j = 3,4)$. The bounded solution of equation (20) and (21) are written as

$$\hat{\psi}_1 = \sum_{i=1}^{2}(Q_i e^{-\lambda_i z}), \tag{22}$$

$$\hat{\varphi} = \sum_{i=1}^{2}(O_i Q_i e^{-\lambda_i z}), \tag{23}$$

$$\hat{\psi}_2 = \sum_{j=3}^{4}(Q_j e^{-\lambda_j z}), \tag{24}$$

$$\hat{\Gamma} = \sum_{j=3}^{4}(O_j Q_j e^{-\lambda_j z}), \tag{25}$$

where, $Q_i (i = 1,2)$, $Q_j (j = 3,4)$ are arbitrary constants, and $O_i (i = 1,2)$, $O_j (j = 3,4)$ are coupling constants, represented defined in Appendix III.

4. Boundary Conditions

The appropriate boundary conditions at $z = 0$ are written as:

$$(i)\quad t_{zz} = G_1(r,t), (ii)\quad t_{zr} = 0, (iii)\quad m_{z\theta} = 0, (iv)\ \varphi = G_2(r,t), \tag{26}$$

where

$$G_1(r,t) = G_{10}H(a-r)\delta(t), \qquad G_2(r,t) = \frac{G_{20}\delta(t)}{2\pi r}\begin{cases} 0, & t \le 0, \\ \frac{t}{t_0}, & 0 < t \le t_0, \\ 1 & t > t_0. \end{cases} \tag{27}$$

Here, G_{10} is magnitude of the force, G_{20} is a constant temperature applied at the boundary surface, t is time, $\delta(\ )$ is Dirac-delta function and H () is known as Heaviside step function.

Employing the transforms defined by (17)- (18) on (26) - (27), we get:

$$(i)\ \hat{t}_{zz} = \hat{G}_1(\chi,p), (ii)\ \hat{t}_{zr} = 0,\ (iii)\ \hat{m}_{z\theta} = 0, (iv)\ \hat{\varphi} = \hat{G}_2(\chi,p), \text{at } z = 0 \tag{28}$$

where

$$\hat{G}_1(\chi,p) = G_{10}\frac{aJ_1(\chi a)}{\chi}, \quad \hat{G}_2(\chi,p) = G_{20}\frac{(1-e^{-pt_0})}{2\pi t_0 p^2}. \tag{29}$$

Substituting the values of $\hat{\psi}_1, \hat{\varphi}, \hat{\psi}_2$ and $\hat{\Gamma}$ from (22)-(25) in the boundary conditions (28) with the conditions (9), (14)-(16), (17)-(19) after some algebraic simplifications, we obtain the components of displacement, stresses, tangential couple stress, conductive temperature, and thermodynamic temperature as follows

$$\hat{u}_r = \frac{-\chi}{\Delta}\left[\sum_{i=1}^{2}(\hat{G}_1(\chi,p)\Delta_{i1} + \hat{G}_2(\chi,p)\acute{\Delta}_{i1})e^{-\lambda_i z} - \sum_{i=3}^{4}(\hat{G}_1(\chi,p)\Delta_{i1} + \hat{G}_2(\chi,p)\acute{\Delta}_{i1})\lambda_i e^{-\lambda_i z}\right], \tag{30}$$

$$\hat{u}_z = \frac{-1}{\Delta}\left[\sum_{i=1}^{2}(\hat{G}_1(\chi,p)\Delta_{i1} + \hat{G}_2(\chi,p)\acute{\Delta}_{i1})\lambda_i e^{-\lambda_i z} - \sum_{i=3}^{4}(\hat{G}_1(\chi,p)\Delta_{i1} + \hat{G}_2(\chi,p)\acute{\Delta}_{i1})\chi^2 e^{-\lambda_i z}\right], \tag{31}$$

$$\hat{t}_{zz} = \frac{1}{\Delta}\left[\sum_{i=1}^{4}\left(\hat{G}_1(\chi,p)\Delta_{i1} + \hat{G}_2(\chi,p)\acute{\Delta}_{i1}\right)U_i e^{-\lambda_i z}\right], \tag{32}$$

$$\hat{t}_{zr} = \frac{1}{\Delta}\left[\sum_{i=1}^{4}\left(\hat{G}_1(\chi,p)\Delta_{i1} + \hat{G}_2(\chi,p)\acute{\Delta}_{i1}\right)U_{i+4} e^{-\lambda_i z}\right], \tag{33}$$

$$\hat{m}_{z\theta} = \frac{1}{\Delta}\left[\sum_{i=3}^{4}\left(\hat{G}_1(\chi,p)\Delta_{i1} + \hat{G}_2(\chi,p)\acute{\Delta}_{i1}\right)U_{i+6} e^{-\lambda_i z}\right], \tag{34}$$

$$\hat{\varphi} = \frac{1}{\Delta}\left[\sum_{i=1}^{2}\left(\hat{G}_1(\chi,p)\Delta_{i1} + \hat{G}_2(\chi,p)\acute{\Delta}_{i1}\right)O_i e^{-\lambda_i z}\right], \tag{35}$$

$$\hat{T} = \frac{1}{\Delta}\left[\sum_{i=1}^{2}\left(\hat{G}_1(\chi,p)\Delta_{i1} + \hat{G}_2(\chi,p)\acute{\Delta}_{i1}\right)O_i U_{i+10} e^{-\lambda_i z}\right], \tag{36}$$

where all symbols are defined in Appendix-IV.

5. Inversion of Transformations

To obtain the solution of the problem in physical domain, we need to invert the transforms as in (30) - (36). Here the displacement components, stresses, tangential couple stress, conductive temperature and thermodynamic temperature are of the form $\hat{f}(\chi, z, p)$. For getting the function $f(r, z, t)$ in the physical domain, we followed Sharma,et.al. [17].

6. Special Cases

i) The above results are reduced for MGT thermoviscoelastic half-space with non-local and HTT parameters when $\alpha = \beta = \gamma = \kappa = 0$ in equations (30)-(36).

ii) If $K^* = 0$ and $\tau_0 = 0$, then corressponding expressions given by equations (30)-(36) have been reduced to micropolar thermoviscoelastic half-space for classical theory with non-local and HTT effects.

iii) Considering $K^* = 0$ in equations (30)-(36), we get results for micropolar thermoviscoelastic medium with one relaxation time along with impacts of non-local and HTT.

iv) The expressions from equations (30)-(36) reduce for micropolar thermoviscoelastic medium witout enegy dissipation along non-local and HTT effects when $K_1^* = 0, K^* \neq 0$ and $\tau_0 = 0$ are considered.

v) If $K_1^* \neq 0, K^* \neq 0$ and $\tau_0 = 0$, then we obtained results from equations (30)-(36) for micropolar thermoviscoelastic half-space with energy dissipation under non-local and HTT effects.

7. Discussion and Implementation of Numerical Solutions

The numerical calculations are carried out for different cases to study the effects of various parameters,

(i) hyperbolic two-temperature (HTT) and viscosity (ii) non-local ξ_1 and ξ_2 parameters, in micropolar thermoviscoelastic medium based on MGT heat equation under normal distributed force and ramp type thermal source.

The following parameters are taken for Magnesium crystal in numerical computations:

Following Eringen [19], the values of micropolar constants are

$$\lambda = 9.4 \times 10^{10}\ \mathrm{Nm^{-2}}, \mu = 4 \times 10^{10}\ \mathrm{Nm^{-2}}, \quad \rho = 1.74 \times 10^{3}\ \mathrm{Kgm^{-3}},$$
$$\hat{j} = 0.2 \times 10^{-19}\mathrm{m^2}, \gamma = 0.779 \times 10^{-9}\mathrm{N}, \kappa = 1.0 \times 10^{10}\mathrm{Nm^{-2}}.$$

Thermal parameters are given by (Dhaliwal and Singh [20]):

$$K_1^* = 1.7 \times 10^{2}\ \mathrm{Ns^{-1}K^{-1}}, C_e = 1.04 \times 10^{10}\mathrm{m^2 s^{-2} K^{-1}}, \tau_0 = 0.02\mathrm{s}, T_0 = 298\ \mathrm{K},$$
$$\alpha_t = 2.36 \times 10^{-6}\mathrm{K^{-1}}.$$

The relevant parameters used for numerical computation can be expressed as
$Q_1 = 0.4s,\ Q_2 = 0.3s,\quad Q_3 = 0.1s,\quad Q_6 = 0.5s.$

7.1. Impact of non-Local parameters

We consider HTT parameter and viscosity parameters for the range $0 \le r \le 3$.
The computation of graphs is as following:
The curves in presence of both non-local parameters ($\xi_1 = 0.75$ and $\xi_2 = 0.25$) with viscosity are represented by solid black line.
The curves in presence of only ξ_1 i.e., ($\xi_1 = 0.75$ and $\xi_2 = 0.0$) with viscosity is represented by big dashed blue line.
The curves in presence of only ξ_2 i.e., ($\xi_1 = 0.0$ and $\xi_2 = 0.25$) with viscosity is represented by small dashed orange line.
The curves in absence of both non-local parameters ($\xi_1 = 0.0$ and $\xi_2 = 0.0$) with viscosity is represented by big dashed pink line with centered symbol circle (o).

7.2. *Normal Force over Circular Region*

Figure 1 illustrates the behavior of t_{zz} vs. r. It is noticed that, the values of t_{zz} shows decreasing trend in the range $0 \le r \le 2$ for all considered cases with a greater decrement for $(\xi_1 = 0.75, \xi_2 = 0.0)$ whereas opposite trend is noticed in magnitude of t_{zz} for $(\xi_1 = 0.0, \xi_2 = 0.0)$ and $(\xi_1 = 0.0, \xi_2 = 0.25)$ compared to $(\xi_1 = 0.75, \xi_2 = 0.25)$ and $(\xi_1 = 0.75, \xi_2 = 0.0)$ respectively, in the remaining range.

Figure 2 is a plot of t_{zr} vs. r. It is evident that t_{zr} follows a similar pattern across all models, with substantial differences in their magnitudes in the range $0 \le r \le 1.75$ whereas reverse behaviour is noticed for $(\xi_1 = 0.0, \xi_2 = 0.0)$ and $(\xi_1 = 0.0, \xi_2 = 0.25)$ compared to $(\xi_1 = 0.75, \xi_2 = 0.25)$ and $(\xi_1 = 0.75, \xi_2 = 0.0)$ respectively, in the remaining range but magnitude of t_{zr} is higher for $(\xi_1 = 0.75, \xi_2 = 0.0)$.

Figure 3 demonstrates that the magnitude of $m_{z\theta}$ decreases in the ranges $0.20 \le r \le 1$, $2.2 \le r \le 3$, while the opposite trend is noticed in the remaining interval for $(\xi_1 = 0.75, \xi_2 = 0.25)$ and $(\xi_1 = 0.75, \xi_2 = 0.0)$. Furthermore, the magnitude of $m_{z\theta}$ is shown mirror image in absence of non-local parameter when compared with $(\xi_1 = 0.0, \xi_2 = 0.25)$ across entire range except some values of r.

Figure 4 exhibits variations of φ vs. r. It is noticed that the magnitude of φ follows similar trend in absence of non-local parameters and presence of non-local parameter ξ_2 only whereas magnitude of φ declines throughout entire range for $(\xi_1 = 0.75, \xi_2 = 0.25)$ and $(\xi_1 = 0.75, \xi_2 = 0.0)$ with significant difference in their magnitudes.

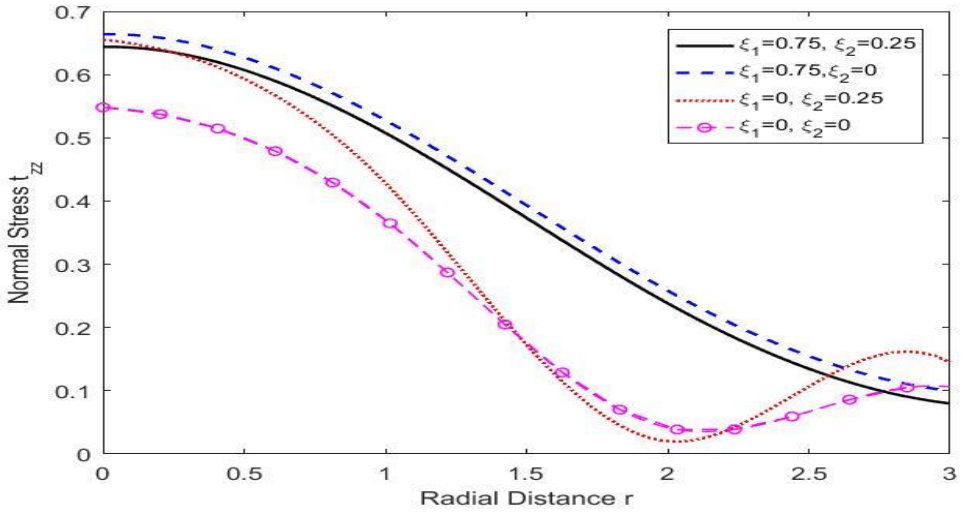

Fig.1 Variation of Normal stress t_{zz} w.r.t. r

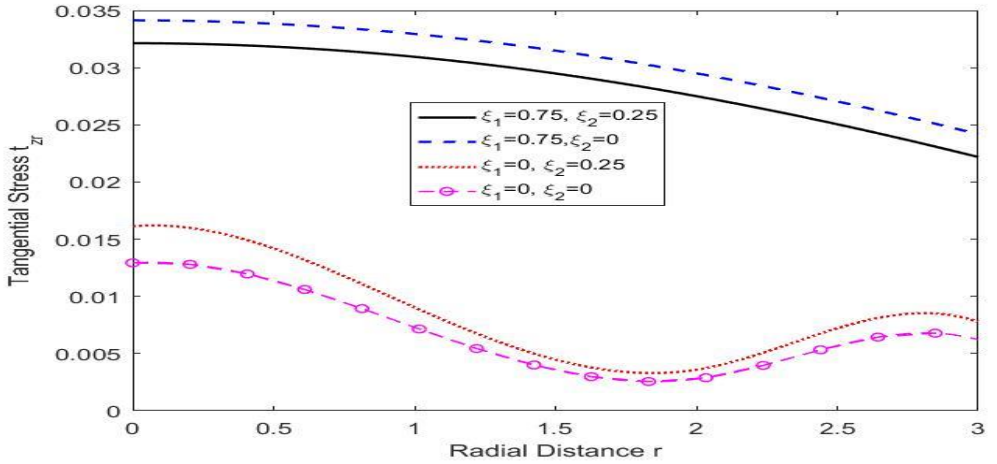

Fig.2 Variation of Tangential stress t_{zr} w.r.t. r

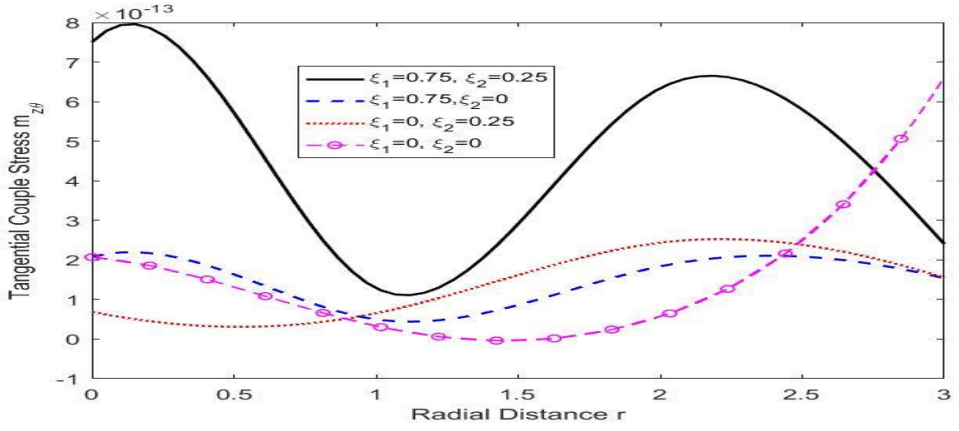

Fig.3 Variation of Tangential Couple stress $m_{z\theta}$ w.r.t. r

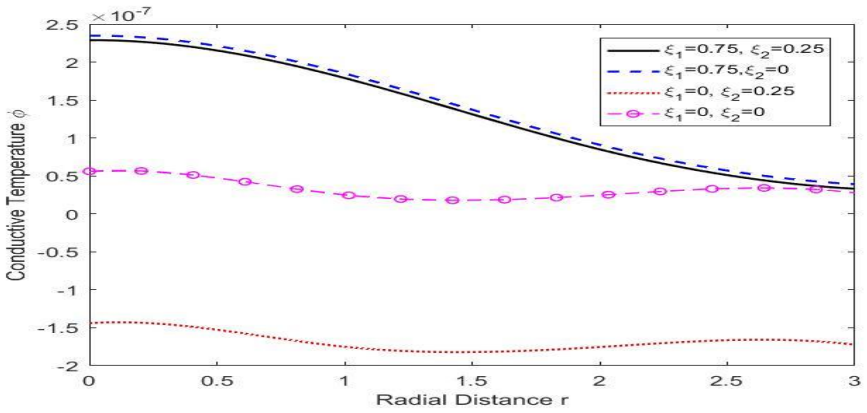

Fig.4 Variation of Conductive temperature ϕ w.r.t. r

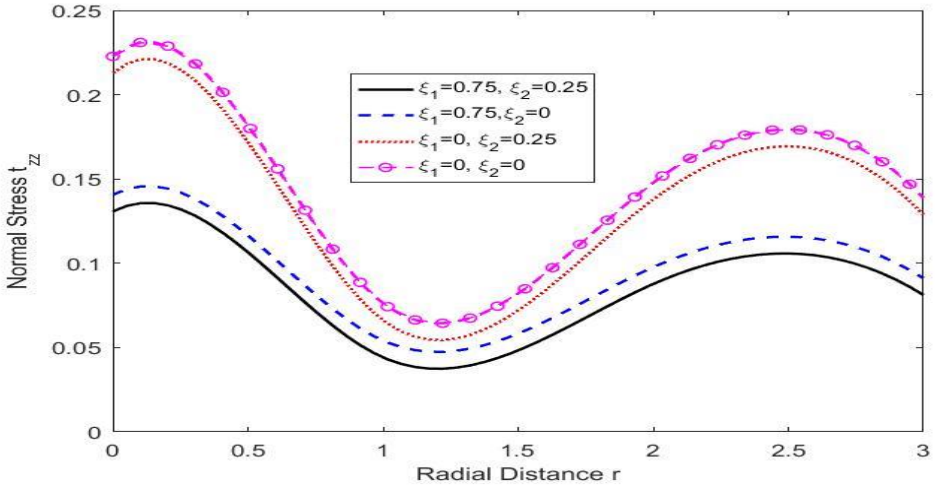

Fig.5 Variation of Normal stress t_{zz} w.r.t. r

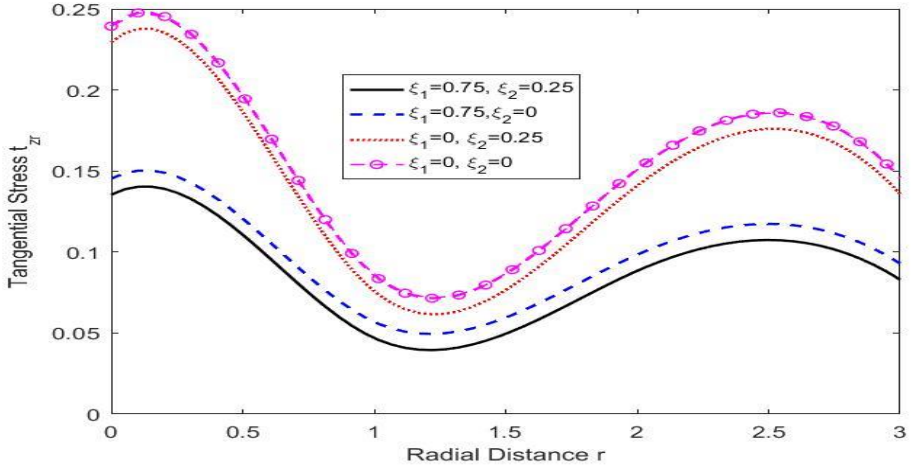

Fig.6 Variation of Tangential stress t_{zr} w.r.t. r

7.3. Concentrated Thermal Source

Figure 5 depicts the behavior of t_{zz} vs. r. It is noticed that close to the loading surface, the magnitude of t_{zz} rises for all examined cases. As r increases, t_{zz} display an oscillatory pattern across all cases, with highest magnitude occurring in absence of non-local parameters.

Figure 6 present variations of t_{zr} vs. r. It is clear that t_{zr} exhibits a trend similar to that of t_{zz} ,though their magnitudes differ significantly.

Figure 7 is a plot of $m_{z\theta}$ vs. r. It is evident that the magnitude of $m_{z\theta}$ decreases witin the intervals $0.20 \leq r \leq 0.25$, $2 \leq r \leq 3$, while the opposite trend is noticed in the remaining interval for all examined cases but magnitude of $m_{z\theta}$ is higher for $(\xi_1 = 0.75, \xi_2 = 0.0)$.

The plot of φ vs. r is illustrated in figure 8. It is noted that although the overall pattern of φ remains consistent across all considered cases but magnitude of φ is lowest when non-local parameter ξ_1 is absent

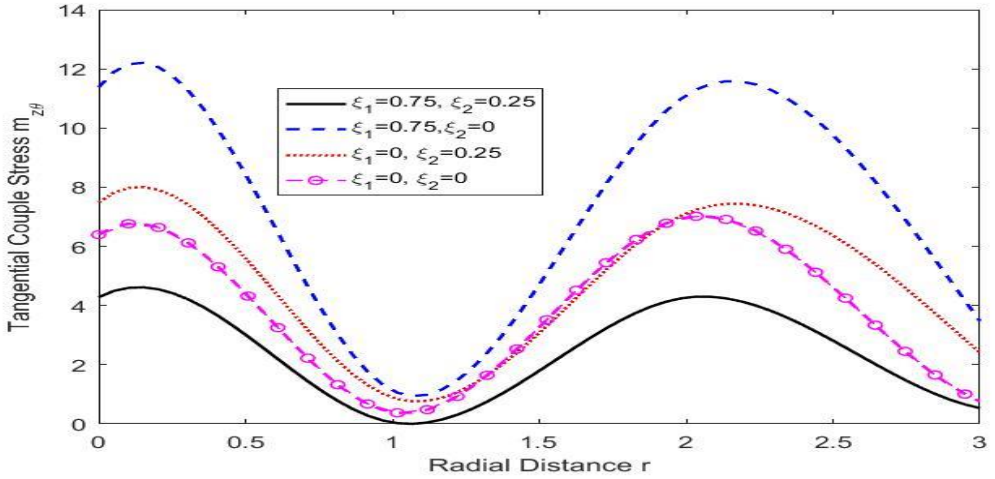

Fig.7 Variation of Tangential Couple stress $m_{z\theta}$ w.r.t. r

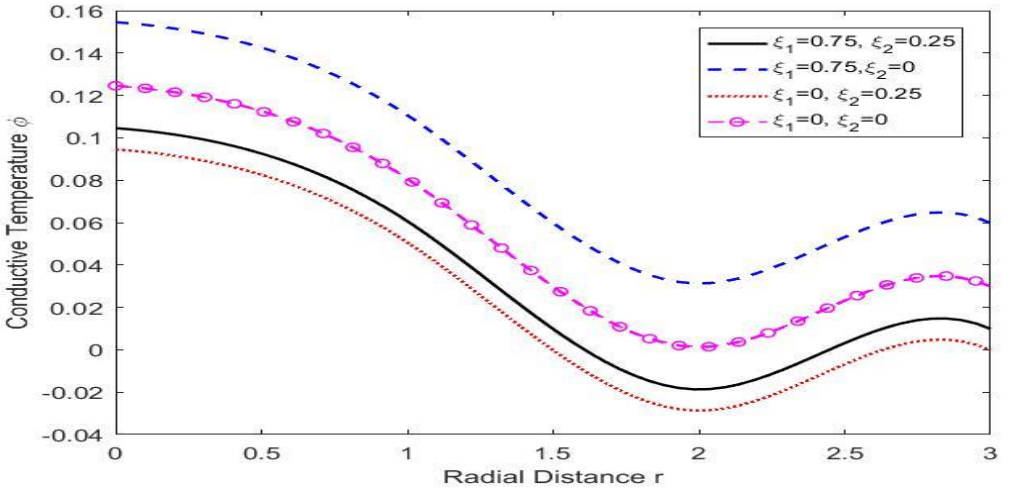

Fig.8 Variation of Conductive temperature ϕ w.r.t. r

7.4. Impact of HTT and Viscosity

We take non-local parameters $\xi_1 = 0.75$ and $\xi_2 = 0.25$ for the range $0 \leq r \leq 3$. The computation of graphs is as following:

- In presence of HTT with viscosity is represented by solid black line **(WVHT)**.
- In presence of HTT without viscosity parameters is represented by big dashed blue line **(WOVHT)**.

- In absence of HTT with viscosity parameters is represented by small dashed orange line **(WVT)**.
- In absence of HTT without viscosity parameters is represented by big dashed pink line with centered symbol circle (o) **(WOVT)**.

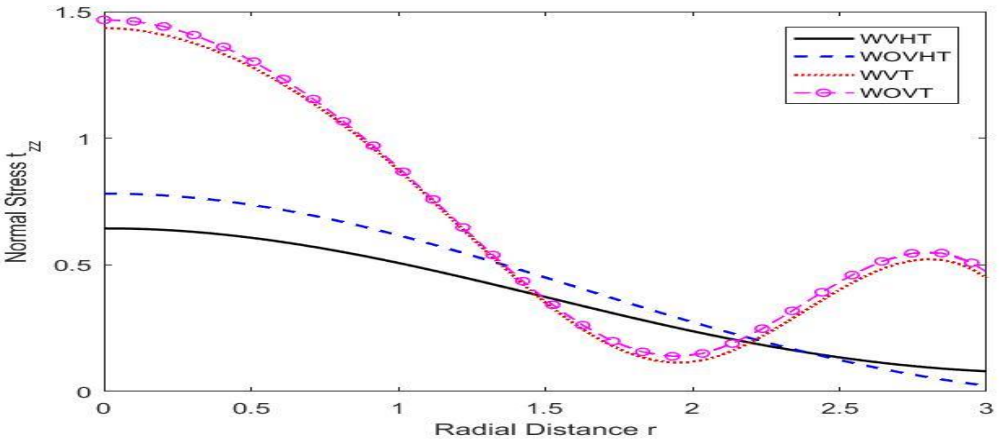

Fig.9 Variation of Normal stress t_{zz} w.r.t. r

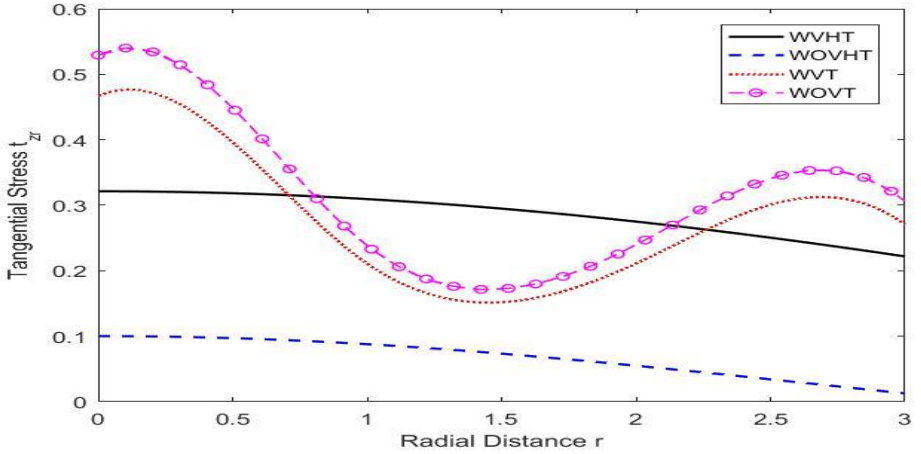

Fig.10 Variation of Tangential stress t_{zr} w.r.t. r

7.5. Normal Force over Circular Region

Figure 9 depicts the variations of t_{zz} vs. r. It is noticed that, for all considered cases the magnitude of t_{zz} decreases within the interval $0 \leq r \leq 2$ whereas beyond this range an increasing trend is noted attributed to the absence of HTT parameter.

Figure 10 presents the of plot of t_{zr} vs. r. It is evident that t_{zr} exhibits an oscillatory trend for WVT and WOVT cases, while a descending trend is seen for WVHT and WOVHT.

Figure 11 depicts the variations of $m_{z\theta}$ vs. r. It is noticed that presences of HTT parameter, causes $m_{z\theta}$ to display an opposite trend in WVHT and WOVHT cases when compared to WVT and WOVT, specifically within the range $0 \leq r \leq 1$. Beyond this range, all cases sxhibits a similar pattern.

Figure 12 illustrate the behavior of φ vs. r. The magnitude of φ follows an oscillatory pattern with an overall decreasing trend all across cases, with the WOVT case depicting lowest magnitude.

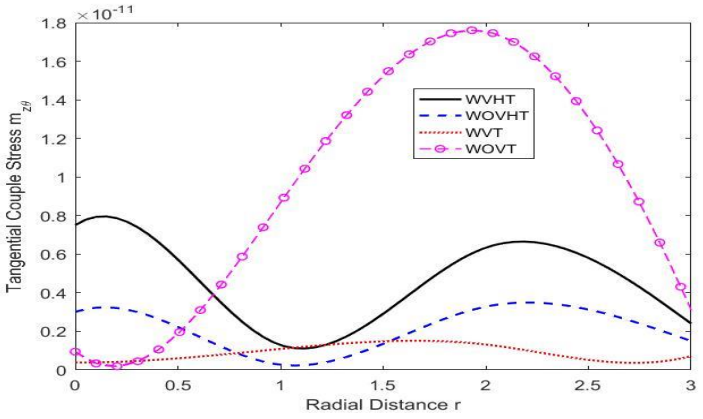

Fig.11 Variation of Tangential Couple stress $m_{z\theta}$ w.r.t. r

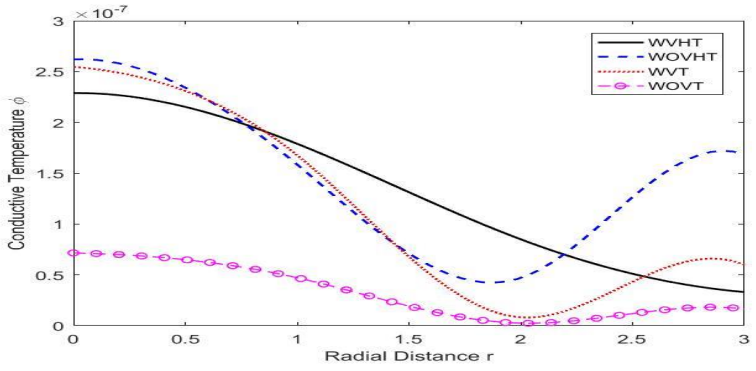

Fig.12 Variation of Conductive temperature ϕ w.r.t. r

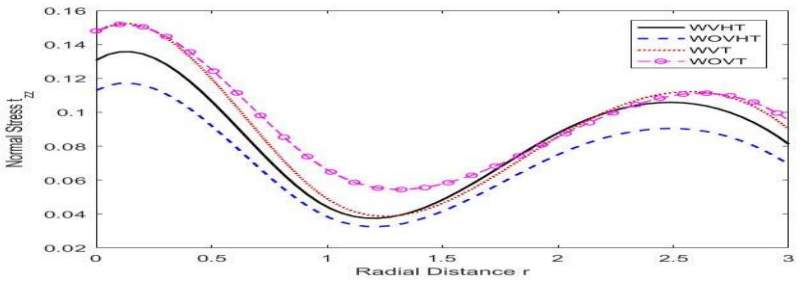

Fig.13 Variation of Normal stress t_{zz} w.r.t. r

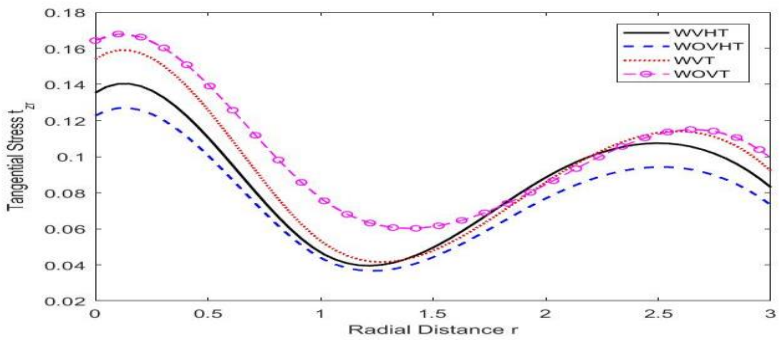

Fig.14 Variation of Tangential stress t_{zr} w.r.t. r

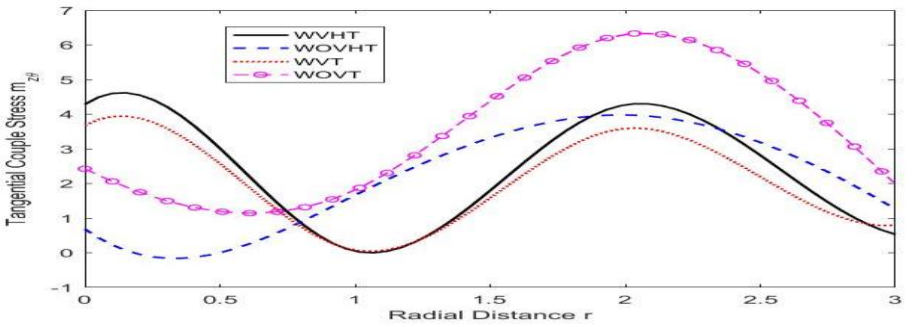

Fig.15 Variation of Tangential Couple stress $m_{z\theta}$ w.r.t. r

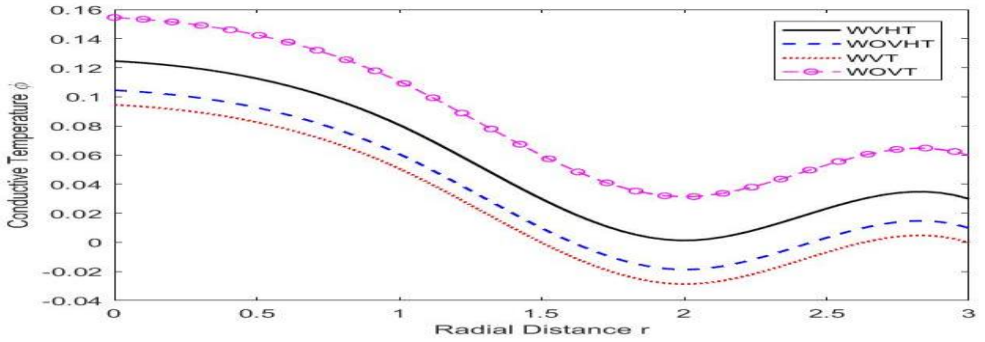

Fig.16 Variation of Conductive temperature ϕ w.r.t. r

7.6. Concentrated Thermal Source

Figure 13 displays how t_{zz} varies with radial displacement. Near the loading surface, its magnitude initially increases and then exhibits oscillatory behaviour for all considered scenarios as radial displacement increases.

Figure 14 presents the variation of t_{zr} versus radial displacement. Although all cases follow a similar trend, the magnitude t_{zr} is found to be lowest for the WOVHT case.

Figure 15 shows the variation of $m_{z\theta}$ with respect to radial displacement. It is noticed that the magnitude of $m_{z\theta}$ depicts opposite trend for WVHT and WVT when compared with WOVHT and WOVT respectively in the range $0 \leq r \leq 1$, while in the remaining range, all cases exhibit similar trends.

Figure 16 illustrates the distribution of ϕ against r. Although the general pattern remains consistent across all cases, the WVHT configuration results in a higher magnitude of ϕ compared to WOVHT, attributed to the influence of viscosity parameters.

8. Conclusions

This study addresses a two-dimensional axisymmetric problem based on the Moore-Gibson-Thompson (MGT) heat conduction model, incorporating the effects of hyperbolic two-temperature (HTT), non-local, and viscosity parameters. The governing equations are reformulated in a dimensionless framework using appropriate potential functions. These transformed equations are solved analytically through Laplace and Hankel transforms, and the physical field quantities—such as displacement components, stress components, tangential couple stress, conductive temperature, and thermodynamic temperature—are retrieved in the original domain via numerical inversion techniques.

The numerical analysis investigates the influence of HTT, non-locality, and viscosity on the

physical responses under both mechanical loading and thermal excitation. The following observations emerge from the study:

1. The inclusion of non-local effects leads to oscillatory behavior in normal stress, tangential stress, tangential couple stress, and conductive temperature under the application of a thermal source.
2. When a normal force is applied over a circular boundary region, non-local parameters amplify the magnitudes of normal stress, tangential stress, and conductive temperature.
3. In the presence of the HTT parameter, the viscosity term notably enhances the tangential stress and tangential couple stress under mechanical loading.
4. Under thermal loading conditions, the presence of both viscosity and HTT parameters results in elevated values of normal stress, tangential stress, tangential couple stress, and conductive temperature compared to other scenarios.

The significance of this research lies in its application to real-world systems, particularly those involving complex material behavior and structural geometries.The theoretical model developed here offers practical insights relevant to domains such as geomechanics, seismic analysis, soil-structure interactions, and broader applications within the field of micropolar thermoviscoelasticity.

Appendix-I

$$b_1^0=\frac{\lambda_0+\mu_0}{\rho c_1^2}, b_2^0=\frac{\mu_0+\kappa_0}{\rho c_1^2}, \quad b_3^0=\frac{\kappa_0\gamma_1 T_0}{\rho^2 c_1^4}, \quad b_4^0=\frac{\gamma_1 T_0}{\rho c_1^2}, \quad b_5^0=\frac{\gamma_0}{\rho c_1^2 j}, \quad b_6^0=\frac{\kappa_0 c_1^2}{j\gamma_1\omega_1^2 T_0},$$
$$b_7^0=\frac{2\kappa_0}{j\rho\omega_1^2},$$
$$b_8^0=\frac{\gamma_1 c_1^2}{\omega_1 K_1^*}, \quad b_9^0=\frac{K^*}{\omega_1 K_1^*}, \quad b_{10}^0=\frac{(\lambda_0+2\mu_0+\kappa_0)}{\gamma_1 T_0}, \quad b_{11}^0=\frac{\lambda_0}{\gamma_1 T_0}, \quad b_{12}^0=\frac{\mu_0+\kappa_0}{\gamma_1 T_0}, \quad b_{13}^0=\frac{\mu_0}{\gamma_1 T_0},$$

$$b_{14}^0=\frac{\kappa_0}{\gamma_1 T_0}, \quad b_{15}^0=\frac{\gamma_0\omega_1^2}{\rho c_1^4}, \quad \nabla^2=\frac{\partial^2}{\partial r^2}+\frac{1}{r}\frac{\partial}{\partial r}+\frac{\partial^2}{\partial z^2}.$$

Appendix-II

$$D_{01}=\frac{[(b_3\varsigma p^2+p+b_9^0)(\chi^2+b_1)]+b_4[p^2b_3(1+\chi^2\varsigma)+\chi^2(p+b_9^0)]+b_8^0b_3(1+2\chi^2\varsigma)}{b_4(b_3\varsigma p^2+p+b_9^0)+b_8^0b_3\varsigma},$$
$$D_{02}=\frac{(\chi^2+b_1)[p^2b_3(1+\chi^2\varsigma)+\chi^2(p+b_9^0)]+b_3b_8^0\chi^2(1+\chi^2\varsigma)}{b_4(b_3\varsigma p^2+p+b_9^0)+b_8^0b_3\varsigma},$$
$$D_{03}=\frac{\left[(b_2^0+p^2{\xi_1}^2)(b_5^0\chi^2+b_7^0+b_2)\right]+\left[(b_5^0+p^2{\xi_2}^2)+(b_2^0\chi^2+b_1)\right]-b_3^0b_6^0}{(b_5^0+p^2{\xi_2}^2)(b_2^0+p^2{\xi_1}^2)},$$
$$D_{04}=\frac{[(b_2^0\chi^2+b_1)(b_5^0\chi^2+b_7^0+b_2)]+b_3^0b_6^0\chi^2}{(b_5^0+p^2{\xi_2}^2)(b_2^0+p^2{\xi_1}^2)},$$
$$b_1=p^2(1+\chi^2\xi_1^2), \quad b_2=p^2(1+\chi^2\xi_2^2), \quad b_3=(1+\tau_0 p), \quad b_4=(1+p^2\xi_1^2).$$

Appendix-III

$$O_i = \frac{\lambda_i^2 b_4 - (\chi^2 + b_1)}{b_4^0(1+\varsigma(\chi^2 - \lambda_i^2))}, \qquad O_j = \frac{(b_2^0\chi^2 + b_4) - \lambda_j^2(b_2^0 + p^2\xi_1^2)}{b_3^0}, \qquad (i = 1,2), (j = 3,4).$$

Appendix-IV

$$\Delta = HT_1 + HT_2, \quad HT_1 = -O_1[U_9(U_4U_6 - U_2U_8) - U_{10}(U_3U_6 - U_2U_7)],$$
$$HT_2 = O_2[U_9(U_4U_5 - U_1U_8) + U_{10}(U_1U_7 - U_3U_5)], \quad \Delta_{11} = O_2(U_7U_{10} - U_8U_9),$$
$$\Delta_{21} = O_1(U_8U_9 - U_7U_{10}), \qquad \Delta_{31} = -U_{10}(O_2U_5 - O_1U_6),$$
$$\Delta_{41} = -U_9(O_1U_6 - O_2U_5),$$
$$\acute{\Delta}_{11} = U_2(U_6U_{10} - U_7U_{10} + U_8U_9),$$
$$\acute{\Delta}_{21} = U_1(U_{10}U_7 - U_8U_9) - U_5(U_3U_{10} - U_4U_9),$$
$$\acute{\Delta}_{31} = -U_{10}(U_1U_6 - U_2U_5), \qquad \acute{\Delta}_{41} = U_9(U_1U_6 - U_2U_5),$$
$$U_i = (b_{10}^0\lambda_i^2 - (1 + \varsigma\chi^2)O_i + \varsigma O_i\lambda_i^2 - \chi^2 b_{11}^0),$$
$$U_j = \chi^2\lambda_j(b_{11}^0 - b_{10}^0), \qquad U_{i+4} = \chi\lambda_i(b_{12}^0 + b_{13}^0),$$
$$U_{j+4} = -\chi(b_{12}^0\lambda_j^2 + \chi^2 b_{13}^0 + b_{14}^0 O_j),$$
$$U_{j+6} = b_{15}^0\chi\lambda_j O_j, \quad U_{i+10} = (1 + \varsigma(\chi^2 - \lambda_i^2)), \quad (i = 1-2), (j = 3-4).$$

References

[1] P. J. Chen, M. E. Gurtin, On a theory of heat conduction involving two temperatures, 1968.

[2] P. J. Chen, M. E. Gurtin, W. O. Williams, On the thermodynamics of non-simple elastic materials with two temperatures, *Zeitschrift für angewandte Mathematik und Physik ZAMP,* Vol. 20, No. 1, pp. 107-112, 1969/01/01, 1969.

[3] H. M. Youssef, Theory of two-temperature-generalized thermoelasticity, *IMA Journal of Applied Mathematics,* Vol. 71, No. 3, pp. 383-390, 2006.

[4] H. M. Youssef, A. A. El-Bary, Theory of hyperbolic two-temperature generalized thermoelasticity, *Mater. Phys. Mech,* Vol. 40, No. 2, pp. 158-171, 2018.

[5] A. Hobiny, I. Abbas, M. Marin, The Influences of the Hyperbolic Two-Temperatures Theory on Waves Propagation in a Semiconductor Material Containing Spherical Cavity, *Mathematics,* Vol. 10, No. 1, pp. 121, 2022.

[6] A. C. Eringen, D. Edelen, On nonlocal elasticity, *International journal of engineering science,* Vol. 10, No. 3, pp. 233-248, 1972.

[7] A. C. Eringen, Linear theory of micropolar elasticity, *Journal of Mathematical Mechanics,* Vol. 15, No. 6, pp. 909-923, 1966.

[8] M. Marin, Weak Solutions in Elasticity of Dipolar Porous Materials, *Mathematical Problems in Engineering,* Vol. 2008, No. 1, pp. 158908, 2008.

[9] K. Sharma, M. Marin, Reflection and transmission of waves from imperfect boundary between two heat conducting micropolar thermoelastic solids, *Analele Stiintifice ale Universitatii Ovidius Constanta, Seria Matematica,* Vol. 22, pp. 151-175, 06/01, 2014.

[10] R. Quintanilla, Moore–Gibson–Thompson thermoelasticity, *Mathematics and Mechanics of Solids,* Vol. 24, pp. 108128651986200, 07/21, 2019.

[11] M. Marin, On existence and uniqueness in thermoelasticity of micropolar bodies, *Comptes rendus de l'Académie des Sciences Paris, Série II,* Vol. 321, No. 12, pp. 375-480, 1995.

[12] S. Sharma, S. Khator, Power generation planning with reserve dispatch and weather uncertainties including penetration of renewable sources, *International Journal of Smart Grid and Clean Energy*, pp. 292-303, 01/01, 2021.

[13] S. Sharma, S. Khator, Micro-Grid Planning with Aggregator's Role in the Renewable Inclusive Prosumer Market, *Journal of Power and Energy Engineering,* Vol. 10, No. 4, pp. 47-62, 2022.

[14] M. Marin, On weak solutions in elasticity of dipolar bodies with voids, *Journal of Computational and Applied Mathematics,* Vol. 82, No. 1, pp. 291-297, 1997/09/15/, 1997.

[15] A. Zeeshan, M. I. Khan, R. Ellahi, M. Marin, Computational Intelligence Approach for Optimising MHD Casson Ternary Hybrid Nanofluid over the Shrinking Sheet with the Effects of Radiation, *Applied Sciences,* Vol. 13, No. 17, pp. 9510, 2023.

[16] A. E. Abouelregal, S. S. Askar, M. Marin, B. Mohamed, The theory of thermoelasticity with a memory-dependent dynamic response for a thermo-piezoelectric functionally graded rotating rod, *Scientific Reports,* Vol. 13, No. 1, pp. 9052, 2023/06/03, 2023.

[17] S. Sharma, M. Marin, H. Altenbach, Elastodynamic interactions in thermoelastic diffusion including non-local and phase lags, *ZAMM - Journal of Applied Mathematics and Mechanics / Zeitschrift für Angewandte Mathematik und Mechanik,* Vol. 105, No. 1, pp. e202401059, 2025.

[18] M. Marin, S. Sharma, R. Kumar, S. Vlase, Fundamental solution and Green's function in orthotropic photothermoelastic media with temperature-dependent properties under the Moore–Gibson–Thompson model, *ZAMM - Journal of Applied Mathematics and Mechanics / Zeitschrift für Angewandte Mathematik und Mechanik,* Vol. 105, No. 6, pp. e70124, 2025.

[19] A. C. Eringen, Plane waves in nonlocal micropolar elasticity, *International Journal of Engineering Science,* Vol. 22, No. 8, pp. 1113-1121, 1984/01/01/, 1984.

[20] R. S. Dhaliwal, A. Singh, 1980, *Dynamic Coupled Thermoelasticity*, Hindustan Publishing Corporation,